

# PCCP

Accepted Manuscript



This is an *Accepted Manuscript*, which has been through the Royal Society of Chemistry peer review process and has been accepted for publication.

*Accepted Manuscripts* are published online shortly after acceptance, before technical editing, formatting and proof reading. Using this free service, authors can make their results available to the community, in citable form, before we publish the edited article. We will replace this *Accepted Manuscript* with the edited and formatted *Advance Article* as soon as it is available.

You can find more information about *Accepted Manuscripts* in the [Information for Authors](#).

Please note that technical editing may introduce minor changes to the text and/or graphics, which may alter content. The journal's standard [Terms & Conditions](#) and the [Ethical guidelines](#) still apply. In no event shall the Royal Society of Chemistry be held responsible for any errors or omissions in this *Accepted Manuscript* or any consequences arising from the use of any information it contains.

## Gold Nanoparticle Embedded in Silica Hollow Nanospheres Induced by Compressed CO<sub>2</sub> as an Efficient Catalyst for Selective Oxidation

Li Guo, Ran Zhang, Chen Chen, Jizhong Chen, Xiuge Zhao, Angjun Chen, Xuerui Liu, Yuhe Xiu, Zhenshan Hou\*

Key Laboratory for Advanced Materials, Research Institute of Industrial Catalysis, East China University of Science and Technology, Shanghai, 200237, China.

E-mail: houzhenshan@ecust.edu.cn

Metal nanoparticles embedded in hollow materials are important due to their wide application in catalysis. In this work, we disclosed a nontraditional synthetic pathway to prepare silica hollow nanospheres by hydrothermal treatment in the presence of compressed CO<sub>2</sub>. Especially, the silica hollow nanospheres with outer diameter of about 16 nm and inner pore size of 7 nm were obtained with 1.0 MPa CO<sub>2</sub>. The formation mechanism of silica hollow nanospheres induced by CO<sub>2</sub> was investigated by high-pressure UV/Vis spectra. Moreover, gold nanoparticles (2.5 nm) embedded in the silica hollow nanospheres were prepared by one-pot synthesis using HAuCl<sub>4</sub> as a precursor. The current synthetic route of nano-catalyst was simple and facile, in which no etching agent was needed in the process of the hollow material preparation. Besides, this nano-catalyst showed an excellent catalytic performance in epoxidation of styrene with high conversion (82.2%) and selectivity (90.2%) toward styrene oxide, as well as the selective oxidation of ethylbenzene with conversion (26.6%) and selectivity (87.8%) toward acetophenone. Moreover, the Au nanoparticles (AuNPs) embedded in silica hollow nanospheres exhibited an excellent recyclability in both of oxidation reactions.

**Keywords:** Carbon dioxide; Gold Nanoparticle; Hollow silica; Nanospheres; Oxidation;

## 1 Introduction

Hollow structured micro- or nanoscopic spheres have attracted great attention for various applications including catalysis,<sup>1,2</sup> drug delivery,<sup>3</sup> energy storage,<sup>4</sup> and environmental protection.<sup>5</sup> Among hollow structured nanomaterials, silica material is fascinating owing to its outstanding properties, such as prominent mechanical and thermal stability,<sup>6</sup> low toxicity and high biocompatibility.<sup>7</sup> The templating methods for synthesis of silica hollow nanospheres could be roughly classified into hard-templating methods and soft-templating methods. In the conventional hard-templating methods, solid rigid particles are employed as the core template and these can be easily removed through calcination, dissolution, or etching after the formation of shells around the cores.<sup>8-10</sup> The soft-templating methods usually employ surfactant-based micelle/microemulsion as the templates for simultaneously building silica shell and hollow interior by the co-assembly of the surfactant and sol-gel derived silica.<sup>11,12</sup> Although both of these methods are very useful to fabricate silica hollow nanospheres, the preparation processes seem to be complicated and time consuming. Therefore, developing a facile and quick synthesis method to prepare silica hollow spheres remains a great challenge to materials scientists.

On the other hand, it has been well demonstrated that the encapsulation of functional nanoparticles in hollow materials can effectively enhance the stability of these nanoparticles and prevent nanoparticles from sintering. In this aspect, the designing of the yolk-shell structured nanoreactors have received much attention for catalytic applications.<sup>13-15</sup> Nano-gold catalysts have attracted considerable attention in recent years, and have shown unprecedented ability to catalyze a large list of useful chemical reactions such as coupling reaction, hydrogenation, selective oxidation of alcohol, and olefin epoxidation.<sup>16-20</sup> Among them, olefin epoxidation is of great significance in the laboratory as well as in the chemical industry because epoxides are widely used as raw materials for epoxy resins, paints, surfactants, which are important intermediates in organic synthesis.<sup>21</sup> However, Au nanoparticles (AuNPs)-based catalysts are synthesized either as supported nanocatalysts with no shells around them, or with strongly bound self-assembled monolayer shells composed of organic groups

such as alkanethiols and alkylamines.<sup>22,23</sup> Whereas in the former method, the AuNPs usually aggregate during the catalysis process and thus result in gradual deactivation, in the latter case the AuNPs' surfaces are less accessible to reactants and the introduction of alkanethiols and alkylamines are actually negative for the catalytic activity. Normally, the complicated procedures have to be adopted to allow uniform distribution of AuNPs on the support. In order to overcome these drawbacks, Haruta and Claus report gold nanoparticles on silica by using chemical vapor deposition (CVD) with expensive Au complex precursor.<sup>24,25</sup> York-shell microspheres containing a single Au nanoparticle core and a mesoporous silica microspheres are synthesized by employing polystyrene-co-poly (4-vinylpyridine) microspheres as both template to fabricate the hollow mesoporous silica microspheres through sol-gel process and scaffold to immobilize the Au nanoparticle.<sup>26</sup> Up to now, the uniform distribution of AuNPs embedded in silica hollow nanoparticles by one-pot synthesis have rarely reported.

Nowadays, especially with the development of green chemistry, using the unconventional solvent such as supercritical CO<sub>2</sub> or compressed CO<sub>2</sub>, which is usually regarded as green solvent, has attracted much attention. Most importantly, the compressed CO<sub>2</sub> is quite soluble in many liquids, and the dissolution of CO<sub>2</sub> in liquids can change the properties of the liquid solvents considerably.<sup>27</sup> Therefore, compressed CO<sub>2</sub> has been successfully applied in colloid science, such as enhancing the stability of vesicles,<sup>28</sup> switching the transition between different surfactant aggregates.<sup>29</sup>

Keeping in mind the above discussion and our previous research on the catalytic oxidation by Au NPs,<sup>30,31</sup> in this work, we develop a novel and facile strategy to synthesize silica hollow materials and Au nanoparticles embedded in the silica hollow nanoparticles by one-pot method without using etching, swelling or precipitating agent. In comparison with other methods, the significant advantages of this new approach are presented as following: a) the silica shells and the embedded Au nanoparticles were formed simultaneously; b) the introduction of CO<sub>2</sub> can induce and swell the micelle structure, which meant that the usage of traditional swelling agent could be avoided;<sup>32</sup> c) the hydrolysis and condensation of tetraethoxysilane (TEOS)

can be promoted by proton dissociated form carbonic acid in-situ produced from CO<sub>2</sub> and water. Finally, the resulting material was an efficient catalyst for styrene epoxidation and ethyl benzene oxidation with tert-butyl hydroperoxide or molecular oxygen as an oxidant.

## 2 Experimental

### 2.1 Materials.

All materials are of analytical grade and used as received without any further purification. Tetraethoxysilane (TEOS), tert-butyl hydroperoxide (65% TBHP in water), ethylbenzene (EB), styrene, ethanol, 2,6-di-tert-butyl-4-methylphenol (BHT), sulfuric acid, potassium sulphate, sodium 4-(4-dimethylaminophenylazo) benzenesulphonate (MO), and chloroauric acid were obtained from Shanghai Chemical Reagent Inc. of the Chinese Medicine Group. The triblock copolymer poly(ethylene glycol)-poly(propylene glycol)-poly(ethylene glycol) (Pluronic F127) and pyrene were purchased from Sigma-Aldrich. CO<sub>2</sub> was supplied by Shanghai Shangnong Gas Factory with a purity of >99.995%. Silica gel (SiO<sub>2</sub>) was obtained from Qingdao Marine Chemical Co., Ltd., China. Deionized water with a resistivity of 18 MΩ cm was used in all experiments.

### 2.2 Characterization.

X-ray diffraction (XRD) patterns were collected on a D/MAX 2550 VB/PC diffractometer with Cu K radiation. Nitrogen sorption isotherms were measured using a Micromeritics ASAP 2020M system. The samples were degassed for 10 h at 200 °C before the measurement. Scanning electron microscopy (SEM) experiments were performed on JSM electron microscopes (JEOL JSM-6360LV, Japan). Transmission electron microscopy (TEM) experiments were performed on a JEOL JEM 2100 transmission electron microscope operating at 200 kV with nominal resolution of 0.25 nm. High pressure UV/Vis measurements were performed on a Varian Cary 500 spectrophotometer. The apparatus was composed mainly of a temperature-controlled high-pressure UV cell, a gas cylinder, a high-pressure syringe pump (DB-80, made by

Beijing Satellite Manufacturing Factory), and a pressure gauge with an accuracy of  $\pm 0.02$  MPa. For the determination of UV/Vis spectra of MO, 10  $\mu\text{L}$  MO aqueous solution ( $3 \text{ mmol L}^{-1}$ ) was added into the high-pressure cell which contained 3 ml aqueous solution of F127 (1.6 wt%) and  $\text{K}_2\text{SO}_4$  ( $0.33 \text{ mol L}^{-1}$ ) in accordance with the synthetic condition. Then  $\text{CO}_2$  was added into the sample cell until the desired pressure was reached. After  $\text{CO}_2$  pressure remained unchanged, the UV/Vis spectra at different  $\text{CO}_2$  pressures were recorded accordingly. The apparatus and procedures to study the UV/Vis spectra of the pyrene in the aqueous solution of F127 (1.6 wt%) and  $\text{K}_2\text{SO}_4$  ( $0.33 \text{ mol L}^{-1}$ ) were the same as those used for MO.

### 2.3 Synthesis of silica hollow nanospheres.

In a typical synthesis, 0.40 g of triblock copolymers F127 and 1.40 g of  $\text{K}_2\text{SO}_4$  were dissolved in 24 ml of deionized water at  $15^\circ\text{C}$ , and the solution was stirred for 1 h, followed by the addition of 1.66 g of TEOS. The mixtures were sealed in a 100 ml stainless steel autoclave and then pressurized with  $\text{CO}_2$  by high-pressure pump. After stirring 24 h at  $15^\circ\text{C}$ , the mixtures were then hydrothermally treated in the static condition at  $100^\circ\text{C}$  for another 24 h. The white solid precipitate was separated by filtering, washed with deionized water and ethanol several times, and dried at  $60^\circ\text{C}$  overnight. Calcination of the samples were performed at  $550^\circ\text{C}$  in air for 5 h with the ramp rate of  $1^\circ\text{C}/\text{min}$  to obtain white powders as HS- $\text{CO}_2$ -x, where x represented the pressure of  $\text{CO}_2$  at  $15^\circ\text{C}$ . In addition, 0.40 g of triblock copolymers F127 and 1.40 g of  $\text{K}_2\text{SO}_4$  were dissolved in 23.3 ml  $\text{H}_2\text{O}$ , and then pH of the solution was adjusted to 3.6 by adding  $4 \text{ mol L}^{-1}$   $\text{H}_2\text{SO}_4$ . The resulting material ( $\text{SiO}_2$ -S) was obtained by following similar procedure with that of the synthesis of HS- $\text{CO}_2$ -x.

### 2.4 Synthesis of Au nanoparticles embedded in the silica hollow nanospheres

The synthesis procedures are similar to that of silica hollow nanospheres described above except that  $\text{HAuCl}_4 \cdot 4\text{H}_2\text{O}$  is introduced initially. A mixed solution containing F127 (0.40 g), water (24 ml),  $\text{K}_2\text{SO}_4$  (1.40 g), and  $\text{HAuCl}_4 \cdot 4\text{H}_2\text{O}$  (0.01 g) was stirred using a magnetic bar at  $15^\circ\text{C}$  for 1 h and then 1.66 g TEOS was added,

followed by pressurizing with CO<sub>2</sub>. After 24 h, the mixture was directly hydrothermally treated in the static condition at 100 °C for another 24 h. After cooling and depressurizing, the light pink solid products were separated by filtration, washed with deionized water and ethanol several times. The as-synthesized materials were subsequently subjected to extraction using ethanol by soxhlet extractor. After removing of the surfactant and drying at 40 °C in vacuum oven overnight, the products were then reduced at 150 °C for 1 h by H<sub>2</sub> to obtain as Au@HS-CO<sub>2</sub>-x (0.45g, Yield: 91%). 0.77 wt% of Au in the silica hollow nanospheres was found by ICP-AES analysis, indicating almost all of HAuCl<sub>4</sub> precursor was embedded into silica hollow nanospheres. Additionally, a high Au loading Au-1.7@HS-CO<sub>2</sub>-1 catalyst (1.7 wt% Au in silica hollow nanospheres) was also prepared by using the similar procedure.

For the sake of comparison, HAuCl<sub>4</sub>•4H<sub>2</sub>O (10.5 mg) was dissolved in 50 ml H<sub>2</sub>O, and then impregnated with 0.495 g of silica gel. The pH value of the solution was adjusted to 7 with 1 mol L<sup>-1</sup> NaOH solution. The suspension was stirred at 80 °C for 2 h, then filtered, thoroughly washed with H<sub>2</sub>O and ethanol, and dried in a vacuum oven at 40 °C overnight. The pink powders were then reduced at 150 °C for 1 h by H<sub>2</sub> to afford Au/SiO<sub>2</sub> catalyst. 0.91 wt% of Au was found by ICP-AES analysis.

### 2.5 Typical Procedure for Selective Oxidation.

In a styrene epoxidation reaction, the Au@HS-CO<sub>2</sub>-1 (50 mg) was charged with a solution of styrene (1.3 ml, 10 mmol), TBHP (5.38 g, 36 mmol), and acetonitrile (5 ml) in a round-bottom glass reaction vessel. The solution was stirred at 80 °C in nitrogen for 24 h. In a typical procedure for ethylbenzene oxidation reaction with TBHP as an oxidant, the Au@HS-CO<sub>2</sub>-1 (25 mg) was mixed with a solution of ethylbenzene (0.69 ml, 5.65 mmol), TBHP (2.53 g, 16.95 mmol), and acetonitrile (2.5 ml) in a round-bottom glass reaction vessel. The solution was stirred at 80 °C in nitrogen for 24 h.

For the ethylbenzene oxidation with O<sub>2</sub> as an oxidant, the Au@HS-CO<sub>2</sub>-1 (25 mg) was mixed with solution of ethylbenzene (0.77 ml, 6.30 mmol), TBHP (0.012 g,

0.078 mmol) as an initiator, and acetonitrile (2.8 ml) in a stainless steel reactor of 50 ml equipped with a magnetic stirrer. Then O<sub>2</sub> was charged into the reactor to 0.5 MPa and the reactor was heated to 80 °C. After 24 h, the reactor was placed into ice water and O<sub>2</sub> was released slowly by passing it through a cold trap containing acetonitrile to absorb trace amounts of reactant and product entrained in the O<sub>2</sub>.

After reaction, the reaction products were analyzed by GC-MS (Agilent-6890GC-5973MS, HP-5MS, 30 m×0.25 mm×0.25 μm) and GC (Shimadzu GC-2014, KB-50 capillary column, 30 m×0.32 mm×0.50 μm). For the recycling procedure, the catalyst was separated from the reaction mixture by filtration and then washed with acetonitrile three times. Finally the catalyst was dried at 40°C under vacuum and then used for the next run.

### 3 Results and Discussion

On the basis of understanding the aggregate structure induced by compressed CO<sub>2</sub>, the silica hollow materials were conveniently prepared and regulated by tuning CO<sub>2</sub> pressure. In addition to preparing the silica hollow nanoparticles, we also developed a new method to synthesize Au nanoparticles embedded in the silica hollow nanoparticles by one-pot method and examined their performance in catalytic oxidation.

#### 3.1 Formation of Silica Hollow Nanospheres

On account of the ability to tune the micellization for F127-H<sub>2</sub>O-K<sub>2</sub>SO<sub>4</sub> system by changing CO<sub>2</sub> pressure, the CO<sub>2</sub>-induced micelles can be then used to synthesize the hollow silica materials. As shown in Fig. 1, the TEM images of calcined mesoporous silica materials prepared at different pressure of CO<sub>2</sub> clearly showed that the uniform hollow nanospheres can be obtained around 1.0 MPa. It indicated that the shell thickness of the hollow nanospheres was around 4.5 nm and the inner pore size was 7.0 nm which was obviously larger than the original micellar core of F127 (4.9 nm).<sup>33</sup> The increasing pore size of the micellar core of the CO<sub>2</sub>-induced micelles were likely due to the transfer of some PEO groups from bulk water into the micellar inner core.<sup>34</sup> At the lower CO<sub>2</sub> pressure, the micelles structure were not stable due to

thermodynamic equilibrium between the unimers and the micelles,<sup>35</sup> inducing that the contrast between the core and shell was not clear and most of the silica particles were aggregated. However, there were still some small hollow silica spheres with average diameter 13.5 nm and approximately 3.9 to 5.0 nm of the inner pore size at 0.5 MPa (Fig. 1b). With the increasing of the CO<sub>2</sub> pressure, the compressed CO<sub>2</sub> can induce the micellization of F127 molecules, which showed the coexistence of hydrophobic and hydrophilic domains in the micellar core (Fig. S1 and S2), and thus the uniform hollow nanospheres with average diameter 16.0 nm and inner pore size 7.0 nm can be obtained at 1.0 MPa (Fig. 1c). Unfortunately, slight aggregation has been observed when the pressure of CO<sub>2</sub> increased from 1.0 to 2.0 MPa. However, we can still observe that there were some silica hollow nanospheres with average diameter size 14.0 nm and 12.7 nm, respectively (Fig. 1d and 1e). The inner pore size of HS-CO<sub>2</sub>-1.5 and HS-CO<sub>2</sub>-2.0 ranged roughly from 4.7 to 5.3 nm (Fig. 1d and 1e). The poor structure of hollow silica at higher pressure of CO<sub>2</sub> might be due to that the excess of CO<sub>2</sub> could affect the stability of the micelles.<sup>36</sup> Interestingly, the structure of silica hollow nanospheres can not be generated when H<sub>2</sub>SO<sub>4</sub> was used to adjusted the pH of solution to 3.6 (Fig. 1a), which was closed to that of the H<sub>2</sub>CO<sub>3</sub> in-situ produced from H<sub>2</sub>O and CO<sub>2</sub> at 1.0 MPa.<sup>37</sup> These results indicate clearly that the CO<sub>2</sub>-induced micelles not only provide the weak acidic medium for the catalytic hydrolysis of silane precursor but also induce the aggregate structure of micelle that allowed to obtain the silica hollow nanospheres smoothly.

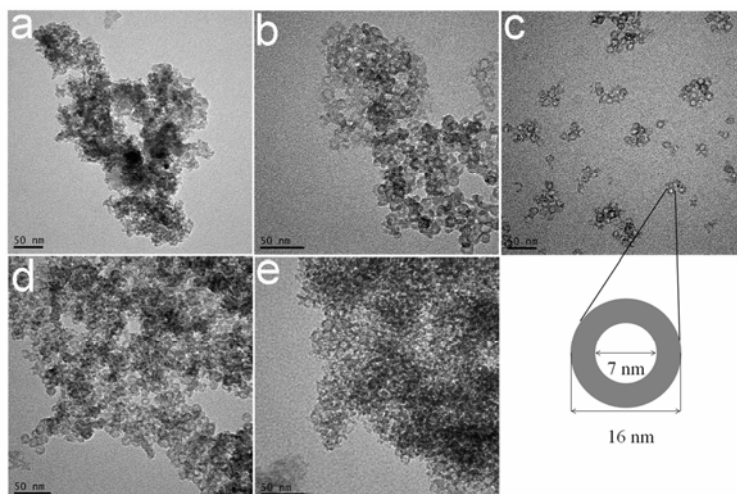


**Fig. 1** TEM images of silica hollow nanospheres under different synthetic conditions: (a) pH value was adjusted to 3.6 with  $\text{H}_2\text{SO}_4$  in the absence of  $\text{CO}_2$ ; (b)-(e):  $\text{CO}_2$  was charged to the different pressures: (b) 0.5 MPa; (c) 1.0 MPa; (d) 1.5 MPa; (e) 2.0 MPa.

Fig. 2 showed the small-angle XRD patterns of calcined mesoporous silica materials prepared at different pressure of  $\text{CO}_2$ . When the pressure increases from 0 to 5.5 MPa, a broad diffraction peak around  $2\theta \sim 0.8^\circ$  appeared only between 0.5 and 2.0 MPa. The small-angle XRD peak was much more shaper, especially when the pressure of  $\text{CO}_2$  reached 1.0 MPa and the HS- $\text{CO}_2$ -1 had a spacing of 11.0 nm between the lattice planes (Fig. 2d), whereas the broad diffraction peak disappeared at higher pressure of  $\text{CO}_2$ . Because the HS- $\text{CO}_2$ -1 showed that the size distribution of the hollow nanospheres was uniform and assembling (Fig. 1c), therefore the small-angle XRD peak arises from closely packed the hollow nanospheres.<sup>38</sup> However, the small-angle XRD peak became weaker or disappeared when the hollow structure are damaged (Fig. 2e-h). On the other hand, there was also no broad diffraction peak appeared when  $\text{H}_2\text{SO}_4$  was used to adjust the pH to 3.6 (Fig. 2a), which proved that only changing the pH can not induce the formation of micellization structure to obtain the silica hollow nanospheres.

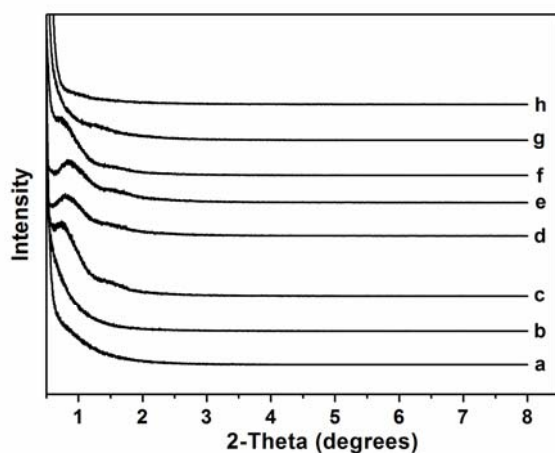


**Fig. 2** Small-angle XRD patterns at different synthesis condition (a) pH value was adjusted to 3.6 with  $\text{H}_2\text{SO}_4$  in the absence of  $\text{CO}_2$  ( $\text{SiO}_2$ -S); (b)-(h):  $\text{CO}_2$  was charged up to the different pressures: (b) 0 MPa; (c) 0.5 MPa; (d) 1.0 MPa; (e) 1.5 MPa; (f)

2.0 MPa; (g) 3.0 MPa; (h) 5.5 MPa CO<sub>2</sub>.

The textural properties of the hollow silica nanospheres were examined by N<sub>2</sub> adsorption-desorption isotherms (Fig. 3). Fig. 3A (b-e) shows type IV isotherms of mesoporous materials. Among all samples shown in Table S1, the HS-CO<sub>2</sub>-0.5 shows the smallest BET surface area (365.7 m<sup>2</sup> g<sup>-1</sup>) but higher average pore size (18.1 nm), which can be described to that only small amount of hollow silica spheres existed and most of them are irregular packing from the TEM image as shown in Fig. 1b. In contrast, the HS-CO<sub>2</sub>-1 has the highest surface area 517.1 m<sup>2</sup> g<sup>-1</sup>, compared to other materials (Table S1). It is noteworthy that there were obviously two capillary condensation steps in the adsorption isotherm at the 1.0 MPa (Fig. 3A inside), suggesting that these samples have two types of mesoporosity. There was slight difference in the core size determined from the N<sub>2</sub> sorption characterization (6.3 nm) and TEM image (7.0 nm) may be due to the fact that the BJH model is not very suitable for measuring the sizes of cage-like pores (Fig. 3B (c)).<sup>40</sup> Furthermore, the pore size distribution of the other materials prepared at the elevated CO<sub>2</sub> pressure was also shown in the Fig. 3B. With the increasing of the CO<sub>2</sub> pressure, the irregular packing pores became larger when compared with SiO<sub>2</sub>-S. The average pore diameter increases from 15.9 nm to 23.2 nm and the simultaneous enlarging of the pore volume from 1.20 cm<sup>3</sup> g<sup>-1</sup> to 1.49 cm<sup>3</sup> g<sup>-1</sup> when the pressure of CO<sub>2</sub> increasing from 1.0 MPa to 2.0 MPa (Table S1). However, there was a slight decline of inner void of the hollow nanospheres from 6.3 nm to 5.0 nm by N<sub>2</sub> adsorption-desorption isotherms (Fig. 3B (c-e)), which was in agreement with TEM results from 7.0 nm to 4.7 nm (Fig. 1c-e). On the other hand, there was only one capillary condensation step in the sample prepared by using H<sub>2</sub>SO<sub>4</sub> (Fig. 3a). The pore size centered at 9.1 nm can be ascribed to the irregular packing pores when using H<sub>2</sub>SO<sub>4</sub> to modify the pH, which was in agreement with the TEM result that there is irregular packing of nanoparticles (Fig. 1a). On the basis of discussion above, the hollow structure can not be attained at lower pressures of CO<sub>2</sub>, or by using H<sub>2</sub>SO<sub>4</sub>, which were in agreement with that of TEM characterization. In contrast, the inner void of the hollow nanospheres becomes

apparent when the pressure of CO<sub>2</sub> increased to 1.0 MPa, and they almost remains (5.0 nm) above 1.0 MPa CO<sub>2</sub> pressure (Fig. 3d and 3e), which was consistent with the image of TEM (Fig. 1), although the slight aggregation has been observed.

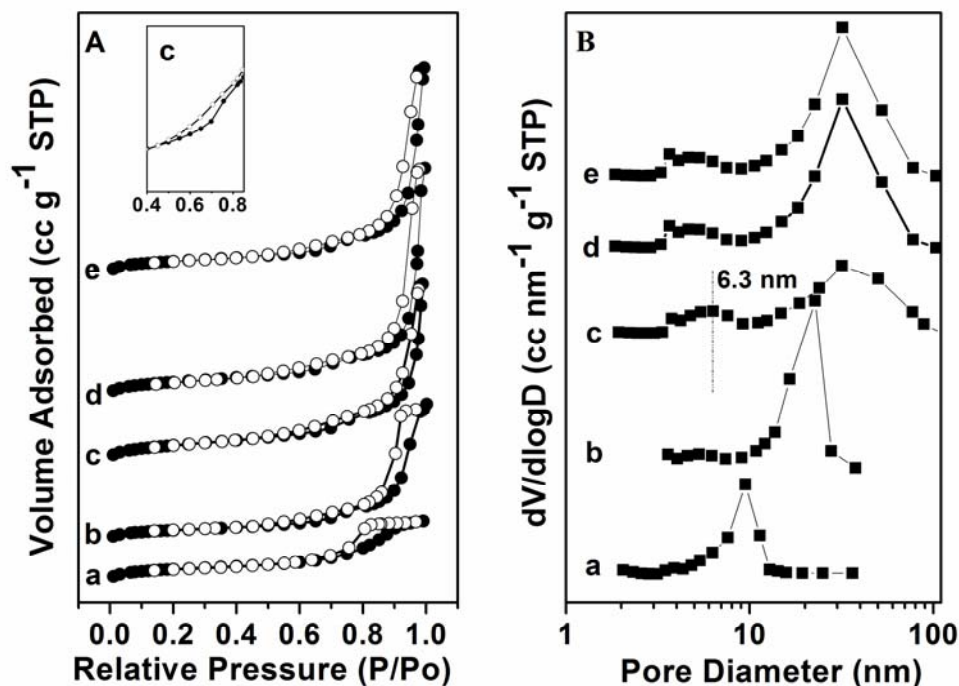


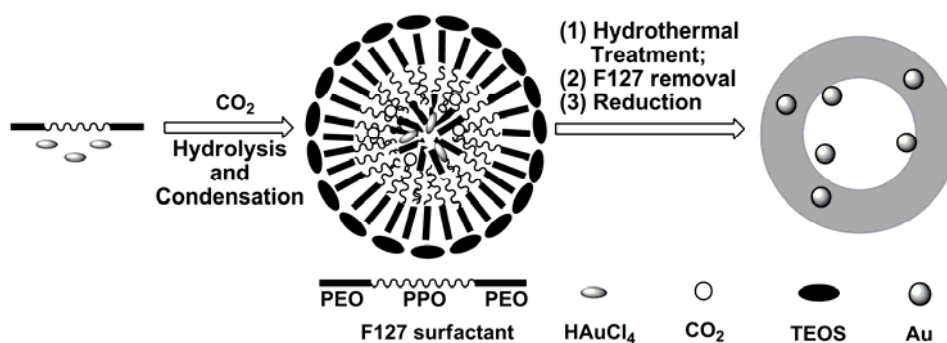
**Fig. 3** (A) Nitrogen adsorption (●) and (○) desorption isotherms (inset is the enlarged part of isotherm (c) at  $P/P_0$  from 0.40 to 0.85) and (B) pore size distribution curves of hollow silica prepared at different pressure of CO<sub>2</sub>. (a) The pH was adjusted to 3.6 with H<sub>2</sub>SO<sub>4</sub> in the absence of CO<sub>2</sub> (SiO<sub>2</sub>-S); (b)-(e): CO<sub>2</sub> was charged to the different pressures: (b) 0.5 MPa; (c) 1.0 MPa; (d) 1.5 MPa; (e) 2.0 MPa.

### 3.2 Gold Nanoparticles Embedded in Silica Hollow Nanospheres

As we have known, because the hollow Au@SiO<sub>2</sub> nanoreactor is normally prepared by chemical etching process, it is not easy to produce small catalytically active nanoparticles (<10 nm) inside the hollow structure.<sup>41</sup> Further taking into account of the amphiphilic core induced by CO<sub>2</sub>, HAuCl<sub>4</sub> was introduced to synthesize Au nanoparticles embedded in silica hollow nanospheres. Regarding the formation of silica hollow nanospheres, the AuNPs embedded in silica hollow nanospheres were obtained through the CO<sub>2</sub>-induced micelles. The formation of Au

nanoparticles embedded in the hollow silica spheres is shown in Scheme 1. The first step involves in the formation of the CO<sub>2</sub>-induced micelles, which have the amphiphilic core. As reported elsewhere, CO<sub>2</sub> has previously been found to modify micellization of Pluronic surfactants.<sup>29,42</sup> In the 1.6 wt% F127 solution (CMC of F127 solution was 0.7 wt%), the core-corona structure could be formed in which a spherical core composed of PPO was surrounded by a corona composed of the strongly hydrated PEO.<sup>33,43</sup> In the present work, the influence of CO<sub>2</sub> pressure on the micelle structure has been investigated by high-pressured UV/Vis spectra using sodium 4-(4-dimethylaminophenylazo) benzenesulphonate (MO) and pyrene as molecular probe. As the pressure continued to increase, the  $\lambda_{\max}$  of MO was gradually blueshifted and a new absorption centered at 396.0 nm appeared (Fig. S1). It is well known that the adsorption maximum  $\lambda_{\max}$  of MO is sensitive to the polarity of its local environment, and the  $\lambda_{\max}$  shifts to shorter wavelength as the polarity decreases.<sup>44</sup> The  $\lambda_{\max}$  of MO decreased from 425.3nm to 396.0 nm as the pressure of CO<sub>2</sub> increased from 0 to 1.0 MPa, which implied that the MO existed in a more hydrophobic domain, but when the pressure of CO<sub>2</sub> increases further, no visible change of the  $\lambda_{\max}$  was observed (Fig. S1). In this case, part of MO molecules might transfer from the interfacial layer of the hydrated PEO into the micellar inner core, most likely due to the formation of a hydrophilic domain in the micellar core, which was also in agreement with that reported by Han's group.<sup>34</sup> On the other hand, the solubilization of the hydrophobic probe molecule pyrene in the 1.6 wt% F127 solution was also investigated by high-pressured UV/Vis spectra. The results under different CO<sub>2</sub> pressures are shown in Fig. S2. In the absence of CO<sub>2</sub>, the absorbance of pyrene is low. With the addition of CO<sub>2</sub> below 0.5 MPa, no visible change of the absorbance of pyrene occurred (Fig. S2 (a-c)). When the pressure of CO<sub>2</sub> was increased continuously, its absorbance increased sharply up to 1.0 MPa. Nevertheless, with pressure of CO<sub>2</sub> increasing further, the absorbance did not show much difference (Fig. S2 (d-f)), which was also consistent with that obtained from the  $\lambda_{\max}$  changes of MO shown as Fig. S1. The solubilization of hydrophobic pyrene is due to the presence of a hydrophobic domain, which indicated that the CO<sub>2</sub> can insert into the micelle core and

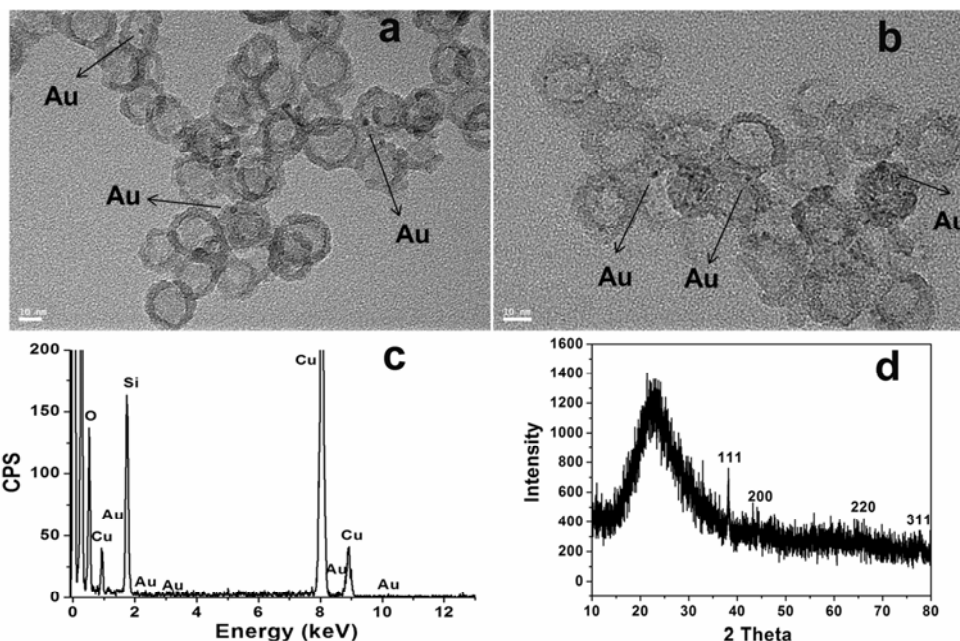
then swell hydrophobic core region. Based on the characterization of UV/Vis spectra, it is suggested that there coexisted hydrophobic and hydrophilic domains in the micellar core, and the hydrophobic micellar core was swollen significantly due to the introduction of CO<sub>2</sub>. In the next step, sol-gel polymerization of TEOS occurs at the surface of the CO<sub>2</sub>-induced micelles (Scheme 1). At the same time, CO<sub>2</sub> can be swollen into the micellar interior and also there is a Lewis acid-base interaction between PEO blocks and inner CO<sub>2</sub>,<sup>45</sup> which provided the driving force for the transfer of some PEO blocks from water into the micellar core. Au species can be distributed inside micelles because of coordinate or stabilize effect by PEO blocks.<sup>46</sup> Finally, following shrinkage of silicate shell and ripening processes during the hydrolysis and condensation of TEOS, and then after remove the surfactant and reduction the Au nanoparticles embedded structures are obtained.



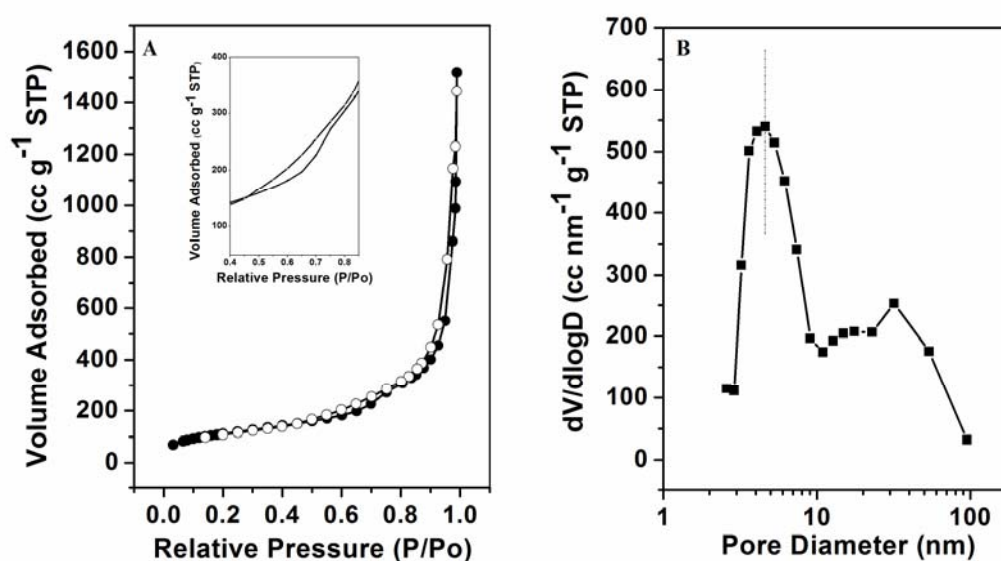
**Scheme 1.** Proposed formation mechanism of Au@HS-CO<sub>2</sub>-1

Fig. 4a showed the TEM image of the silica materials obtained in the CO<sub>2</sub>-induced micelles. The Au@HS-CO<sub>2</sub>-1 nanoparticles showed very small Au nanoparticles (about 2.5 nm) inside the hollow structure. The most of Au nanoparticles (above 95%) was encapsulated into the shell or inside of hollow silica nanospheres, as observed from TEM image (Fig. 4a). However, as HAuCl<sub>4</sub> was solubilized inside the core of micelles randomly, it seemed that Au nanoparticles were not distributed uniformly into hollow silica nanospheres. The presence of AuNPs in the silica hollow nanoparticles was also proved by energy-dispersive X-ray spectrometry (Fig. 4c). Wide-angle XRD measurements display typical broadened diffraction peaks (38.2°) assigned to the Au (111) (Fig. 4d). The N<sub>2</sub>

adsorption-desorption isotherms and pore size distribution of Au@HS-CO<sub>2</sub>-1 display that the BET surface area (401.8 m<sup>2</sup> g<sup>-1</sup>) and pore size (4.6 nm) showed a little decreasing after the introduction of Au inside the hollow materials (Fig. 5), resulting from some Au nanoparticles embedded into the silica hollow nanoparticles.



**Fig. 4** TEM images of Au@HS-CO<sub>2</sub>-1 (a) before reaction, (b) after reaction, (c) EDX of the Au@HS-CO<sub>2</sub>-1, (d) wide-angle XRD pattern of Au@HS-CO<sub>2</sub>-1.



**Fig. 5** (A) Nitrogen adsorption (●) and (○) desorption isotherms (inset is the enlarged

part of isotherm (c) at  $P/P_0$  from 0.40 to 0.85) and (B) pore size distribution curves of Au@HS-CO<sub>2</sub>-1.

### 3.3 Catalytic Performance

In the next step, the as-obtained Au@HS-CO<sub>2</sub>-1 was utilized as a catalyst for the epoxidation of styrene using tert-butylhydroperoxide (TBHP) as an oxidant under nitrogen atmosphere. Besides, Au/SiO<sub>2</sub> was also prepared and the textural properties of Au/SiO<sub>2</sub> were showed in Fig. S3 and S4. As shown in Fig. 6A, the conversion of styrene over Au/SiO<sub>2</sub> is faster than that of Au@HS-CO<sub>2</sub>-1 at the beginning of the reaction, which gave further evidence that most of the Au NPs were embedded in the silica hollow nanoparticles.<sup>47</sup> Both the Au/SiO<sub>2</sub> and Au@HS-CO<sub>2</sub>-1 can reach about 80% conversion of styrene at 24 h, but the selectivity of epoxidation over the Au/SiO<sub>2</sub> decreased sharply as the time is prolonged (Fig. 6B) owing to over-oxidation and benzaldehyde as a by-product. Whereas the Au@HS-CO<sub>2</sub>-1 still showed excellent selectivity to styrene oxide even after a reaction time of 24 h. The excellent selectivity of the Au@HS-CO<sub>2</sub>-1 may stem from well-confined small Au nanoparticles embedded in the silica hollow nanoparticles. If the Au nanoparticles were deposited on the surface of the supported such as Au/SiO<sub>2</sub>, it was easily aggregated to form larger Au nanoparticles (Fig. S3 (b)), which has no significant effect on the conversion, but the selectivity of epoxidation decreased considerably (Table 1, entry 7). Furthermore, a higher loading Au-1.7@HS-CO<sub>2</sub>-1 catalyst afforded a similar conversion (84.1 %) but much lower selectivity (61.9 %) under the same reaction condition. A higher Au loading resulted in the obvious aggregation of Au nanoparticles and partial Au nanoparticles were distributed on the outside of the surface (Fig. S5). Thus it showed similar catalytic performance as that of Au/SiO<sub>2</sub> (Fig. 6B). The catalytic performance of the Au@HS-CO<sub>2</sub>-1 was also compared with the previously reported supported Au catalysts under similar reaction conditions, which has been list in Table 1. Regarding both of activity and selectivity to epoxide over the different catalysts, the present Au@HS-CO<sub>2</sub>-1 exhibited excellent activity and selectivity to epoxide when compared with the previously reported catalysts.

Compared to the metal oxide-supported Au catalysts like Au-meso- $\text{Al}_2\text{O}_3$  and Au-MgO (entries 4 and 5, Table 1), Au@HS- $\text{CO}_2$ -1 displayed a comparable conversion but an enhanced epoxidation selectivity. It was worth noting that Au-PMO-SBA-15 (entry 1, Table 1) showed comparable catalytic activity with the present Au@HS- $\text{CO}_2$ -1 which had also AuNPs entrapped into the mesoporous channel, but it offered slightly lower selectivity than that of the Au@HS- $\text{CO}_2$ -1 catalyst.<sup>48-50</sup> Although porous  $\text{SiO}_2$ -AuNPs- $\text{SiO}_2$  (entry 6, Table 1) material with big Au NPs (16 nm) showed the highest conversion, the selectivity to epoxide was low. As a result, it seemed that the small Au nanoparticles played a crucial role in enhancing the selectivity regardless of Au loading. Moreover, the Au@HS- $\text{CO}_2$ -1 can be reused at least 3 times without losing the conversion and selectivity (Table 1, entry 3) and the TEM image of the Au@HS- $\text{CO}_2$ -1 after reaction demonstrated that the Au@HS- $\text{CO}_2$ -1 maintained the original morphology (Fig. 4b).

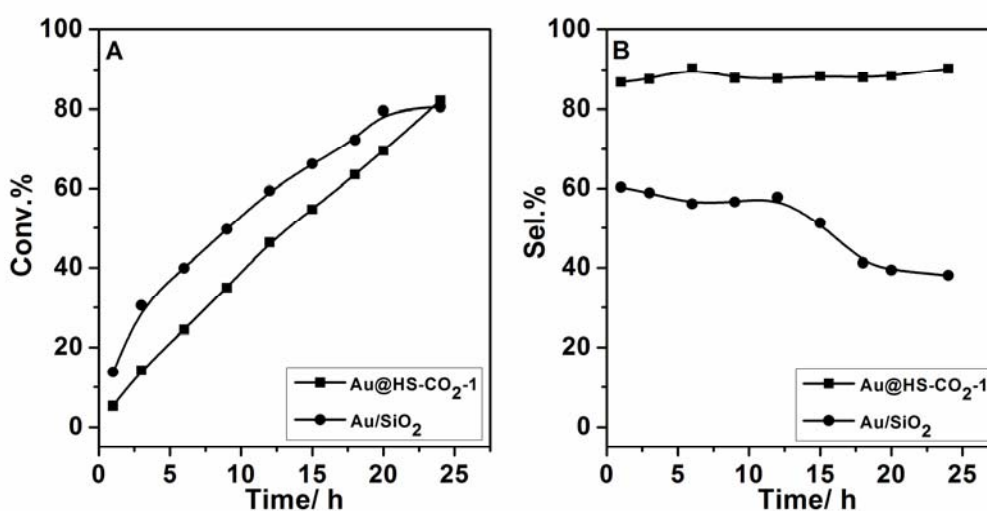


**Fig. 6** (A) The conversion of styrene and (B) the selectivity to styrene oxide at different reaction time (square points represent Au@HS- $\text{CO}_2$ -1 catalyst and triangle points Au/SiO<sub>2</sub>). Reaction conditions: styrene (10 mmol), TBHP (36 mmol), catalyst (50 mg), acetonitrile (5 ml), 353 K, 24 h under Nitrogen. The main side-product was benzaldehyde.

**Table 1.** Epoxidation of styrene catalyzed by gold-based catalysts<sup>a</sup>

Entry	Catalysts	Au loading (wt%)	AuNPs size (nm)	Conv. %	Sel. % <sup>b</sup>	Ref.
1	Au-PMO-SBA-15	2.0	1.8	94.8	75.0	51
2	Au@HS-CO <sub>2</sub> -1	0.76	2.5	82.2	90.2	This work
3	Au@HS-CO <sub>2</sub> -1 <sup>c</sup>	0.76	2.5	81.4	86.2	This work
4	Au-meso-Al <sub>2</sub> O <sub>3</sub>	2.0	3.2	84.3	69.0	49
5	Au-MgO	7.5	7.9	62.6	54.3	50
6	Pores SiO <sub>2</sub> -AuNPs -SiO <sub>2</sub>	0.76	16	100.0	61.0	19
7	Au/SiO <sub>2</sub>	0.91	18	80.6	38.1	This work

<sup>a</sup>These reactions used TBHP as oxidant, temperature was 353 K; <sup>b</sup>Selectivity for styrene oxide; <sup>c</sup>The third run.

Subsequently, Au@HS-CO<sub>2</sub>-1 was further extended to ethylbenzene oxidation, which gave good conversion of ethylbenzene (26.6%) and selectivity (87.8%) toward acetophenone. The main side-product of the oxidation of ethylbenzene was 1-phenylethanol. Although the Au/SiO<sub>2</sub> afforded the similar conversion (21.0%), the selectivity toward acetophenone was only 42.0%. The Au@HS-CO<sub>2</sub>-1 catalyst showed much better activity and selectivity than that of the reported silica-supported silver catalyst at low loading amount of metal.<sup>51</sup> Moreover, the ethylbenzene oxidation was proved to be a free radical mechanism. When BHT was used as a radical inhibitor and added to the reaction mixture, the reaction was completely retarded within 12 h (Fig. S6). Notably, the Au@HS-CO<sub>2</sub>-1 could be recycled at least five times without any loss of activity in the selective oxidation of ethylbenzene (Fig. 7), which implies that Au nanoparticles embedded in the silica hollow nanospheres owned excellent stability. Furthermore, ethylbenzene oxidation can be oxidized selectively with O<sub>2</sub> and a little TBHP as a radical initiator over present Au@HS-CO<sub>2</sub>-1 catalyst, which afforded 28.5% ethylbenzene conversion and 78.5%

selectivity toward acetophenone, demonstrating its universality for the catalysis.

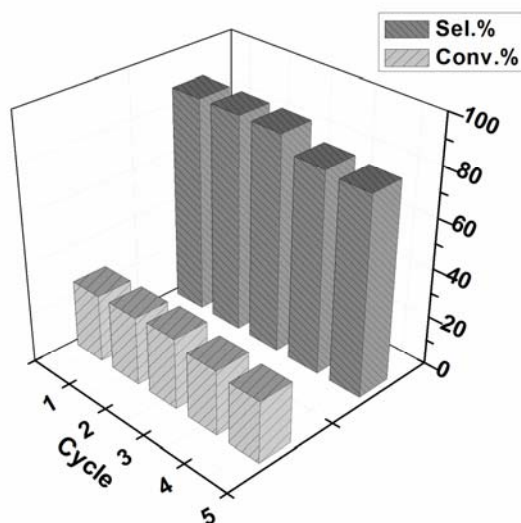


**Fig. 7** The conversion of ethylbenzene and the selectivity toward acetophenone on recycling of the Au@HS-CO<sub>2</sub>-1. Reaction conditions: ethylbenzene (5.65 mmol), TBHP (16.95 mmol), catalyst (25 mg), acetonitrile (2.5 ml), 353 K, 24 h under Nitrogen. The main side-product was 1-phenylethanol.

#### 4 Conclusions

We disclosed a method for preparing new silica hollow nanoparticles based on the CO<sub>2</sub>-induced micelle. This method provides a new pathway to synthesis hollow materials without addition miner acid or swelling agent. Importantly, the preparation of HS-CO<sub>2</sub>-1 avoids using etching agent which is usually used in the synthesis of hollow materials but the etching process is always time-consuming and not a green and efficient synthetic route. Remarkably, when using this method to prepare Au@HS-CO<sub>2</sub>-1, most of the Au NPs were embedded in the hollow silica and showed high activity in selective oxidation. We believe that the materials developed in this work provide excellent future prospects for many applications.

#### Acknowledgements

The authors are grateful for support from the National Natural Science Foundation of China (21373082), innovation Program of Shanghai Municipal Education

Commission (15ZZ031), and the Fundamental Research Funds for the Central Universities.

### Notes and Reference

- (1) X. Yang, L. Du, S. Liao, Y. Li, H. *Catal. Commun.*, 2012, **17**, 29.
- (2) P. M. Arnal, M. Comotti, F. Schuth, *Angew. Chem. Int. Edit.*, 2006, **45**, 8224.
- (3) S. H. Tang, X. Q. Huang, X. L. Chen, N. F. Zheng, *Adv. Funct. Mater.*, 2010, **20**, 2442.
- (4) N. Jayaprakash, J. Shen, S. S. Moganty, A. Corona, L. A. Archer, *Angew. Chem. Int. Edit.*, 2011, **50**, 5904.
- (5) S. W. Liu, J. G. Yu, M. Jaroniec, *J. Am. Chem. Soc.*, 2010, **132**, 11914.
- (6) S. J. Ding, J. S. Chen, G. G. Qi, X. N. Duan, Z. Y. Wang, E. P. Giannelis, L. A. Archer, X. W. Lou, *J. Am. Chem. Soc.*, 2011, **133**, 21.
- (7) Y. F. Zhu, J. L. Shi, W. H. Shen, X. P. Dong, J. W. Feng, M. L. Ruan, Y. S. Li, *Angew. Chem. Int. Edit.*, 2005, **44**, 5083.
- (8) J. Yang, J. U. Lind, W. C. Trogler, *Chem. Mater.*, 2008, **20**, 2875.
- (9) M. Chen, L. M. Wu, S. X. Zhou, B. You, *Adv. Mater.*, 2006, **18**, 801.
- (10) Y. Chen, H. R. Chen, L. M. Guo, Q. J. He, F. Chen, J. Zhou, J. W. Feng, J. L. Shi, *Acs Nano*, 2010, **4**, 529.
- (11) M. H. Yu, H. N. Wang, X. F. Zhou, P. Yuan, C. Z. Yu, *J. Am. Chem. Soc.*, 2007, **129**, 14576.
- (12) Z. G. Feng, Y. S. Li, D. C. Niu, L. Li, W. R. Zhao, H. R. Chen, L. Li, J. H. Gao, M. L. Ruan, J. L. Shi, *Chem. Commun.*, 2008, **23**, 2629.
- (13) S. Ikeda, S. Ishino, T. Harada, N. Okamoto, T. Sakata, H. Mori, S. Kuwabata, T. Torimoto, M. Matsumura, *Angew. Chem. Int. Edit.*, 2006, **45**, 7063.
- (14) X. Q. Huang, C. Y. Guo, L. Q. Zuo, N. F. Zheng, G. D. Stucky, *Small*, 2009, **5**, 361.
- (15) J. Liu, S. Z. Qiao, J. S. Chen, X. W. Lou, X. R. Xing, G. Q. Lu, *Chem. Commun.*, 2011, **47**, 12578.
- (16) A. Wittstock, V. Zielasek, J. Biener, C. M. Friend, M. Baumer, *Science*, 2010,

- 327, 319.
- (17) F. Cárdenas-Lizana, S. Gómez-Quero, H. Idriss, M. A. Keane, *J. Catal.*, 2009, **268**, 223.
- (18) J. Zhu, J. L. Figueiredo, J. L. Faria, *Catal. Commun.*, 2008, **9**, 2395.
- (19) S. Das, T. Asefa, *Top. Catal.*, 2012, **55**, 587.
- (20) J. Liu, F. Wang, S. Qi, Z. Gu, G. Wu, *New J. Chem.*, 2013, **37**, 769.
- (21) K. Weissermel, H.-J. Arpe, *Industrial organic chemistry. John Wiley & Sons*: 2008.
- (22) M. Turner, V. B. Golovko, O. P. H. Vaughan, P. Abdulkin, A. Berenguer-Murcia, M. S. Tikhov, B. F. G. Johnson, R. M. Lambert, *Nature*, 2008, **454**, 981.
- (23) A. Ghosh, C. R. Patra, P. Mukherjee, M. Sastry, R. Kumar, *Microporous Mesoporous Mater.*, 2003, **58**, 201.
- (24) M. Okumura, S. Tsubota, M. Iwamoto, M. Haruta, *Chem. Lett.*, 1998, **27**, 315.
- (25) S. Schimpf, M. Lucas, C. Mohr, U. Rodemerck, A. Bruckner, J. Radnik, H. Hofmeister, P. Claus, *Catal. Today*, 2002, **72**, 63.
- (26) S. Wang, M. Zhang, W. Zhang, *Acs Catal.*, 2011, **1**, 207.
- (27) P. G. Jessop, B. Subramaniam, *Chem. Rev.*, 2007, **107**, 2666.
- (28) W. Li, J. Zhang, S. Cheng, B. Han, C. Zhang, X. Feng, Y. Zhao, *Langmuir*, 2008, **25**, 196.
- (29) W. Li, J. Zhang, Y. Zhao, M. Hou, B. Han, C. Yu, J. Ye, *Chem. Eur. J.*, 2010, **16**, 1296.
- (30) Y. Shi, H. Yang, X. Zhao, T. Cao, J. Chen, W. Zhu, Y. Yu, Z. Hou, *Catal. Commun.*, 2012, **18**, 142.
- (31) C. Chen, H. Yang, J. Chen, R. Zhang, L. Guo, H. Gan, B. Song, W. Zhu, L. Hua, Z. Hou, *Catal. Commun.*, 2014, **47**, 49.
- (32) J. Liu, S. Bai, H. Zhong, C. Li, Q. Yang, *J. Phys. Chem. C.*, 2009, **114**, 953.
- (33) G. Wanka, H. Hoffmann, W. Ulbricht, *Macromolecules*, 1994, **27**, 4145.
- (34) J. Zhang, B. Han, Y. Zhao, J. Li, G. Yang, *Chem. Eur. J.*, 2011, **17**, 4266.
- (35) K. Mortensen, J. S. Pedersen, *Macromolecules*, 1993, **26**, 805.
- (36) Y. Zhao, J. Zhang, Q. Wang, W. Li, J. Li, B. Han, Z. Wu, K. Zhang, Z. Li,

- Langmuir*, 2010, **26**, 4581.
- (37) C. Roosen, M. Ansorge-Schumacher, T. Mang, W. Leitner, L. Greiner, *Green Chem.*, 2007, **9**, 455.
- (38) T. Yokoi, Y. Sakamoto, O. Terasaki, Y. Kubota, T. Okubo, T. Tatsumi, *J. Am. Chem. Soc.*, 2006, **128**, 13664.
- (39) Y. Zhao, J. Zhang, Q. Wang, W. Li, J. Li, B. Han, Z. Wu, K. Zhang, Z. Li, *Langmuir*, 2010, **26**, 4581.
- (40) X. Zhou, S. Qiao, N. Hao, X. Wang, C. Yu, L. Wang, D. Zhao, G. Lu, *Chem. Mater.*, 2007, **19**, 1870.
- (41) X. Wu, L. Tan, D. Chen, X. Meng, F. Tang, *Chem. Commun.*, 2014, **50**, 539.
- (42) W. Li, Y. Yang, T. Luo, J. Zhang, B. Han, *Phys. Chem. Chem. Phys.*, 2014, **16**, 3640.
- (43) I. Goldmints, G.-e. Yu, C. Booth, K. A. Smith, T. A. Hatton, *Langmuir*, 1999, **15**, 1651.
- (44) J. Liu, Y. Ikushima, Z. Shervani, *J. Supercrit. Fluids*, 2004, **32**, 97.
- (45) S. G. Kazarian, M. F. Vincent, F. V. Bright, C. L. Liotta, C. A. Eckert, *J. Am. Chem. Soc.*, 1996, **118**, 1729.
- (46) E. Ploshnik, K. M. Langner, A. Halevi, M. Ben-Lulu, A. H. Müller, J. G. Fraaije, G. Agur Sevink, R. Shenhar, *Adv. Funct. Mater.*, 2013, **23**, 4215.
- (47) H. Y. Liu, L. Y. Zhang, N. Wang, D. S. Su, *Angew. Chem. Int. Edit.*, 2014, **53**, 1.
- (48) D. Yin, L. Qin, J. Liu, C. Li, Y. Jin, *J. Mol. Cat. A: Chem.*, 2005, **240**, 40.
- (49) N. Patil, B. Uphade, P. Jana, S. Bharagava, V. Choudhary, *J. Catal.*, 2004, **223**, 236.
- (50) Y. Jin, P. Wang, D. Yin, J. Liu, H. Qiu, N. Yu, *Microporous Mesoporous Mater.*, 2008, **111**, 569.
- (51) V. Raji, M. Chakraborty, P. A. Parikh, *Ind. Eng. Chem. Res.*, 2012, **51**, 5691.